

Keywords

Pirapora Magnetic Anomaly,
Aeromagnetic surveys,
Spectral analysis,
Thermomagnetism.

Received: December 02, 2018

Accepted: February 26, 2019

Published: March 21, 2019

Thermomagnetic features of Pirapora region, central Brazil

Suze N. P. Guimarães¹, Valiya M. Hamza¹

¹ Department of Geophysics, National Observatory, Rio de Janeiro, Brazil.

Email address

suze@on.br (S. Guimarães)

Corresponding author

Abstract

We report results of a detailed analysis of aeromagnetic survey data of Pirapora region, situated in the São Francisco Craton region, central Brazil. The main residual anomaly is wide, spanning over an area of about 9000 square kilometers, and has a maximum intensity of ± 300 nT. The analytic signal of the anomaly is located between 44.5° and 45.5° W and between 16.5° and 18.5° S and has a maximum value of about 0.028 nTm^{-1} . Results of spectral analysis, based on matched bandpass filtering method, indicate that the anomaly is composed of signals arising from three different layers. The top layer is at depth shallower than 5 km while the intermediate one extends from 5 to 15 km depth. The bottom of deepest magnetic layer extends over depths varying from 20 to 55 km. Along an east-west belt, south of Pirapora anomaly, the depth to bottom of magnetized crust is less than 35 km and comparable to the thickness of the local crust obtained in seismic surveys. However, the thickness of the magnetized crust can exceed 35 km to the north and to the south of the Pirapora anomaly. This implies that the top layer of the mantle itself is magnetized. Results of geothermal model studies indicate Curie isotherm of 580°C may lie at depths greater than 35 km, along wide sections of the Pirapora region, within the São Francisco Craton.

1. Introduction

The magnetic field in the central region of Brazil was investigated since 1970's (Bosum, 1973; Haraly and Hasui, 1985; Marinho, 1993). More recent studies (Borges and Drews, 2001; 2009; Santos, 2006; Borges, 2013) identified in this region the existence of a prominent and wide magnetic anomaly centered in the Pirapora area. Although the Pirapora magnetic anomaly has been studied for several years, there are diverging interpretations on the characteristics and depths of crustal sources responsible for it.

Guimarães et al. (2014) provided results of an integrated analysis of several aeromagnetic data sets and pointed out the advantages of the technique of matched filtering in analysis of magnetic anomalies of crustal origin. Later, Aisengart (2015) interpreted that the source of Pirapora magnetic anomaly may be compatible with that produced by rock types of significantly low values of Curie temperature (different magnetic minerals) and magnetic susceptibility, high degree of remanence and anisotropy. According to this author, a similar case occurs in the Cobar Area, central western New South Wales, Australia (Clark and Tonkins, 1994), where the local magnetic anomaly was associated with the occurrence of pyrrhotite, a mineral associated with nickel and cobalt. In present work, methods of spectral analysis are employed in extracting information on the depths of crustal magnetic

anomalies at Pirapora and neighboring areas. This work also considers implications of the results obtained for the local geothermal field.

2. Geologic Context

The Pirapora region is located in the south-central part of the São Francisco Craton (Almeida, 1977; Almeida et al., 1981). In the southeastern part of this craton (Figure 1) is a segment characterized by basement-involved deformation, syngenetic to tectonic inversion of an intracratonic basin. Within the southeastern part of this basin is a region described as 'Pirapora graben' by Souza Filho, (1995) and also as 'Pirapora aulacogen' by Alkmim et al (2006). In the more recent work of Hercos et al (2008) it is described as 'Pirapora Saliense'. Integration of both seismic and field data allowed identification of three structural domains: a fault-related folds predominance, an extensive monoclinial and undulated, sub-horizontal strata. According to Hercos et al (2008), the deformation rate decreases westward, and the eastern domain shows a dramatic structural relief of about 2500 m resulting from a strong uplift of this portion related to a regional datum. Also, deeper structural investigation around Agua Fria Range shows an inverted half-graben which is limited by a basement high in its western border, designated as Boqueirão High. The easternmost normal fault system of this unit has undergone

weak structural inversion, while the associated covering strata underwent significant shortening as a result of folding related to horizontal displacement. The Boqueirão High formed a rigid buttress that controlled the internal folding/shortening of the syn-rift sequence. The crustal shortening throughout the area is a result of two mechanisms: the inversion of normal faults associated with uplift of the basement blocks, as well as the folding of covering strata enlarged by horizontal forces. The map in Figure 1 illustrates the main tectonic features of São Francisco Craton, where the Pirapora area is located. CODEMIG (2013) provides additional information on the geological characteristics of this region.

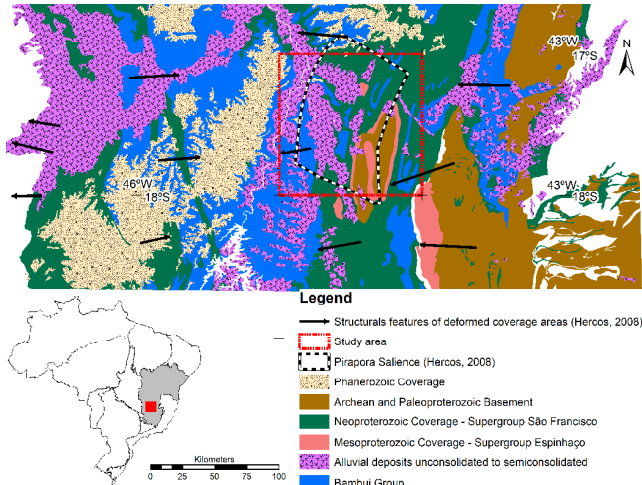


Figure 1 - Map illustrating main tectonic features of the Pirapora region (indicated by the red rectangle) and surrounding areas (Adapted from Alkmim and Marshak, 1998 and Hercos et al, 2008).

3. Aeromagnetic Surveys

The data used in the present work result from the aeromagnetic surveys of the Project 1009 by the Geological Survey of Brazil (CPRM). It was acquired between 1971 and 1972 as part of a geophysical accord between Brazil and Germany. The areas covered by these surveys are shown in Figure 2. Data were acquired initially in analog form and later digitized by Paterson, Grant & Watson Ltd. (PGW) and Western Mining Company (WMC). These digital data sets were made available for academic research by CPRM.

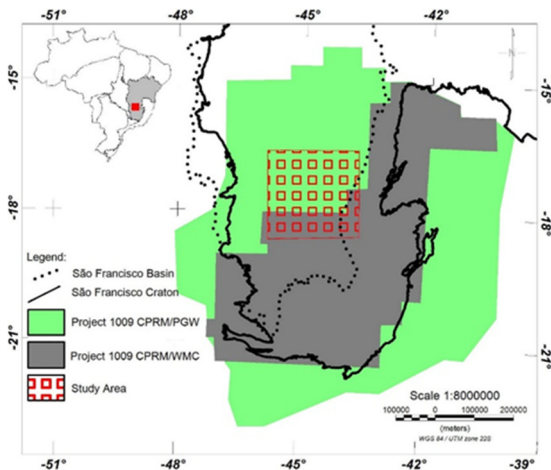


Figure 2 - Map indicating regions covered in aeromagnetic surveys of central Brazil by the Geological Survey of Brazil (CPRM). The study area is indicated with square symbols.

4. Initial Data Analysis

The objective of initial data analysis has been extraction of the anomalous magnetic field from the results of airborne survey results and determination of the depths to top and bottom of the magnetized bodies. Corrections were made by removing the IGRF reference field and the effects of diurnal variations from raw data. The analytic signal was then calculated for determining the characteristics of lateral variations in the anomalous field. This procedure is a linear transformation that highlights the spatial distributions of magnetic sources even at low latitudes, as pointed out by Nabighian (1972), Roest et al (1992) and Phillips (1997). The horizontal derivatives were also calculated, and the results employed for determining the locations of sources present in the anomalous field. These were useful in characterizing linear features (Blakely, 1996; Nabighian et al, 2005). The horizontal derivatives further allowed mapping lateral limits of these sources (Blakely and Simpson, 1986).

5. Residual Field Anomaly

The residual magnetic field at Pirapora, obtained after the initial stage of data reduction, is illustrated Figure 3. The main anomaly is located in an approximately square shaped region, between 43.5° and 45.5° W and 16.5° and 18.5° S. Note that the amplitude of the anomaly varies in the interval of ±300nT and spans over an area of about 9000 square kilometers. Also, several small-scale anomalies occur in the south western parts. The eastern border of the Pirapora area is characterized by extensive positive anomalies with magnitude in excess of 200nT. The northwestern corner is characterized by negative values of less than -100nT.

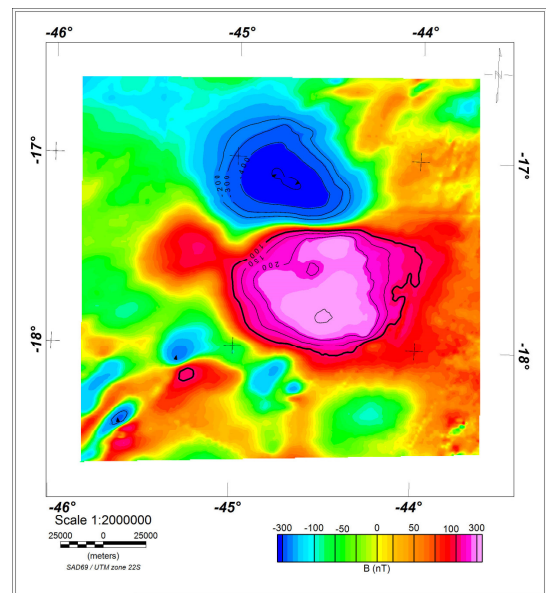


Figure 3 - Map of residual magnetic field in the Pirapora region.

The map of the amplitude of analytic signal, presented in figure 4, provides a better indication of the location of the anomaly. The main anomaly spans over a smaller area and is oval shaped. It is situated in the region, between 44.5° and 45.5° west longitudes and between 16.5° and 18.5° south latitudes. The maximum value of the analytic signal is about 0.028 nTm⁻¹. Notice the presence of several small-amplitude maxima, south of the main anomaly of Pirapora, with values

larger than 0.02 nTm^{-1} . Among the small-amplitude anomalies, the most prominent is located in Três Marias area with an extent of 900 km^2 . The northwestern and south-central parts are characterized by smooth values of the analytic signal, with magnitudes less than 0.007 nTm^{-1} .

Figure 5 illustrates the vertical derivate map of the magnetic field. The shading technique of the map highlights the presence of several prominent lineaments. In the northeastern sector of the Pirapora magnetic anomaly, two lineaments form a V-shaped feature. In the southern sector there is a prominent lineament in the N-S direction, which appears as an offset branch of the N-S lineament in the northern segment outside the region of the anomaly. Other minor lineaments also occur to the southwest of the smaller anomaly at Três Marias and along eastern border of the study area.

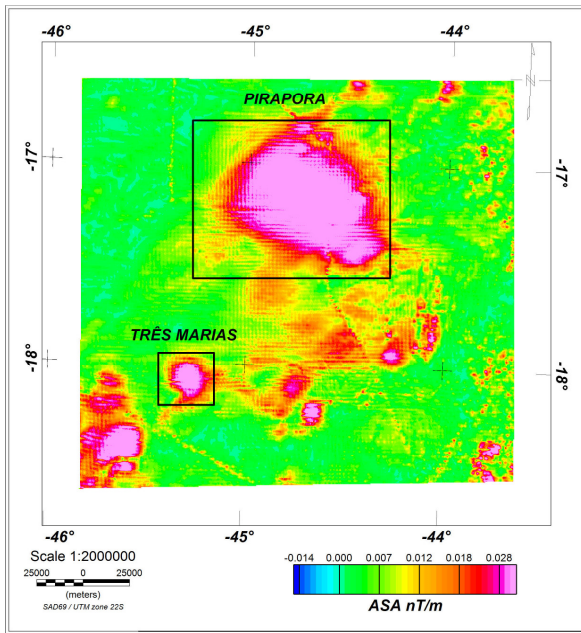


Figure 4 - Distribution of analytic signal amplitude (ASA) of the residual magnetic field in the Pirapora region.

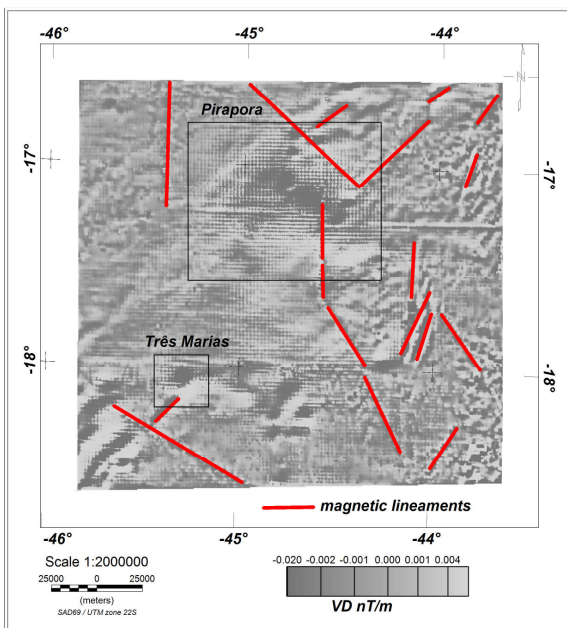


Figure 5 - Distribution of the vertical derivative (VD) of residual magnetic field in the Pirapora region.

6. Spectral Analysis

The techniques of spectral analysis of the residual field were used for the analysis of the magnetic sources at depth. It must be stressed that the spectral peaks in the azimuthally averaged spectra are observed only when sources are randomly magnetized (Spector and Grant, 1970). With uniform magnetization of layers, the spectra have power-law form and no peaks are observed. Guimaraes et al (2014) reported a comparative analysis of two methods used in the spectral estimation of the depth to the bottom of the magnetic layer: the spectral peak method, proposed by Spector and Grant (1970) and the centroid method, originally presented by Bhattacharyya and Leu (1977). The latter estimates the depth of magnetic sources from statistical analysis of magnetic sources and Fourier transform of associated bodies with geometry of regular parallelepiped. Hence, the power density spectrum ($F(k)$) is related to the sources as:

$$|F(k)|^2 = 4 \pi^2 C_m^2 |\theta_m|^2 |\theta_f|^2 M_0^2 e^{-2kz_t} * (1 - e^{-k(z_b - z_t)})^2 S^2(a, b) \quad (1)$$

where k is the wavenumber (cycles/km), C_m a constant, θ_m a factor related to magnetization direction and θ_f a factor related to magnetic field direction. In this equation M_0 is magnetization, z_t and z_b are depths to top and bottom of magnetic sources and $S^2(a, b)$ a factor related to horizontal dimensions of sources. Considering that θ_m and θ_f are radially symmetric the mean value must be a constant. Also, for random magnetization the mean of the radial spectrum ($\Phi_{\Delta T}$) is given by:

$$\Phi_{\Delta T}(|k|) = A e^{-2|k|z_t} (1 - e^{-|k|(z_b - z_t)})^2 \quad (2)$$

For $k \ll z_b - z_t$:

$$\Phi_{\Delta T}(|k|)^{1/2} = C e^{-|k|z_0} \cdot 2d|k| \quad (3)$$

where z_0 is center depth from source or layer anomalous and d is the magnetized layer thickness. Hence, the depth of the bottom magnetized layer (z_b) is given by:

$$Z_b = 2 Z_0 - Z_t \quad (4)$$

It is clear that the slope of the power spectrum for a specific interval is related to the depth of the source. Thus, suitable intervals of spectra were selected, and slopes calculated for each interval.

Guimarães et al (2014) proposed the matched filtering method, which is based on the concept of idealized modeled layers below the observation surface with chosen distribution of magnetization. This method, based on the earlier works of Bhattacharyya and Leu (1977) and Okubo et al (1985), employ the technique proposed by Phillips (1997) where a combination of filters is employed in validating the results of spectral depth computations. The bandpass filter allows the possibility of identifying separate potential-field anomalies from different magnetic layers, considering degree of reliability in data resolution. In the present work, the depth obtained for the top of the layers from this method are used to cross-check the depths obtained from the results of fitting slopes to the amplitude spectrum, in our depth estimation software.

The procedure adopted makes use of the fact that shallowest depth estimate often represents high wavenumber noise and may be discarded unless the magnetic basement is

known to be near the surface. Fitting the slope of the high wavenumber end of the spectrum and removing that component from the spectrum separates the contribution of the topmost layer from the remaining signal. The straight part of the residual spectrum with highest wavenumber is then employed in determination of the depth to the top of the next layer. In this manner, the contribution of successively deeper layers is matched until the steepest slope segment representing the top of the deepest layer is fit.

The radial power spectrum derived from analysis of the Pirapora data is illustrated in Figure 6. Note that the spectral power decreases rapidly with increase in the wavenumber. Thus, in the region of low wave numbers of less than $0.5 \times 10^{-3} \text{ km}^{-1}$ the logarithm of power reaches values in the range of 2 to 6, while at large wavenumbers of more than $0.3 \times 10^{-3} \text{ km}^{-1}$ it falls to values of less than -12. The smoothed curve indicates the fit obtained by matched filtering. For purposes of data analysis, it was found convenient to divide the wave number domains into sectors designated as deep, intermediate and shallow. The lateral boundaries of these sectors are indicated as vertical lines in Figure 6. There are no hard rules for selecting the domains, in view of the uncertainty in spectral data. The deep part is considered as falling in the wave number domain of 0.0 to 0.6, where the power varies from -2 to 6. The intermediate part is considered as falling in the wave number domain of 0.08 to 0.2, where the power varies from -6 to -10. The shallow part is considered as falling in the wave number domain of 0.2 to 0.3, where the power varies from -8 to -12. The part of the spectrum with domain values greater than 0.3 is considered as part of noise in spectral data.

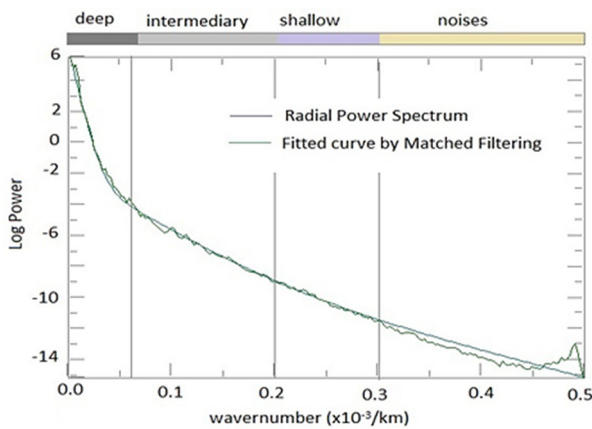


Figure 6 - The radial power spectrum derived from analysis of the magnetic anomaly data of Pirapora. The smooth curve indicates the fit obtained by matched filtering. The vertical lines indicate bounds of wave number domains designated as deep, intermediary and shallow, in the top color bar.

7. Results

The magnetic structure at depth revealed by matched filtering (bandpass filter) may be considered as composed of three layers: shallow, intermediate and deep. The results indicate values of depths to top of these layers of 5, 20 and 30 km respectively. In the analysis based on the spectral peak method for the Pirapora region large windows with dimensions of 200 to 300 km were employed. This choice of window size took into consideration regional extent of the anomalous field in Pirapora, which have dimensions of over 50 km. For practical reasons in the interpretation, the results of the spectral analysis were considered as composed of

blocks, as indicated in Figure 7. Shallow sources are situated at depth interval of 0.7 to 1.4 km. The intermediate sources are situated at depth intervals of approximately 1.1 to 19 km. The deep sources are at depth intervals of 14 to 54 km.

The regional distribution of the blocks of Figure 7 reveals an east-west trending belt where the top of magnetized bodies falls within a relatively narrow range (15-22 km) but depths to the bottom of these bodies fall in the range of 34 to 38 km within the belt. The central points of blocks with depths to bottom of magnetized blocks of less than 40 km have been identified by letters C, B, F and E. These fall along a region where crustal thickness does not exceed estimates obtained by seismic methods (Assumpção et al, 2004; 2013). Hence, such regions may be considered as overlying non-magnetized mantle. However, in regions of blocks A and D, situated north of this belt, the bottom parts of magnetized layers extend to depths greater than 40 km. The approximate outlines of this belt are indicated by black curves in Figure 7.

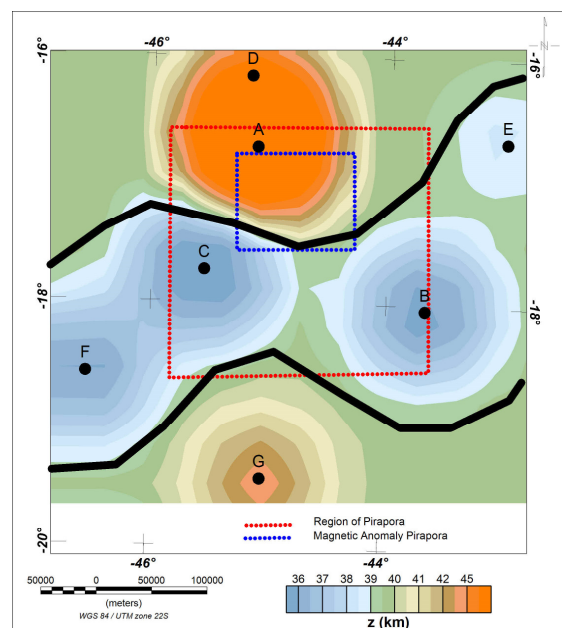


Figure 7 - Distribution of depths to bottom of magnetic sources (DBMS) derived from the spectral magnetic depth determination for the Pirapora region. The black curves delimit the belt where DBMS is limited to crustal layers ($Z_{DBMS} < 40 \text{ km}$). Regions to the north and south of this belt the top layer of the mantle is also magnetized ($Z_{DBMS} > 40 \text{ km}$). The dots indicate centers of sampled windows (cells).

Another notable feature of the region to the north of this belt is that the bottom boundaries of magnetized blocks (D and A) are at larger depths, reaching values of 46 to 53 km. This is also true of Block G, situated in a region to the south of this belt where depth to bottom is 43 km. It implies that top parts of the mantle in regions to the north and south of the east-west trending belt are magnetized. A summary of the results for blocks identified in spectral analysis is presented in Table 1.

The analytic signal of anomalous magnetic fields in block A, associated with sources at shallow and intermediate depths, are illustrated in Figure 8, while those associated with intermediate and deeper depths are illustrated in Figure 9. The anomalous field has sharp boundaries at shallow levels but become diffuse at larger depths. It is clear indication that the contrast between the source region and the surrounding medium is larger at shallow depths compared to that in the middle crust.

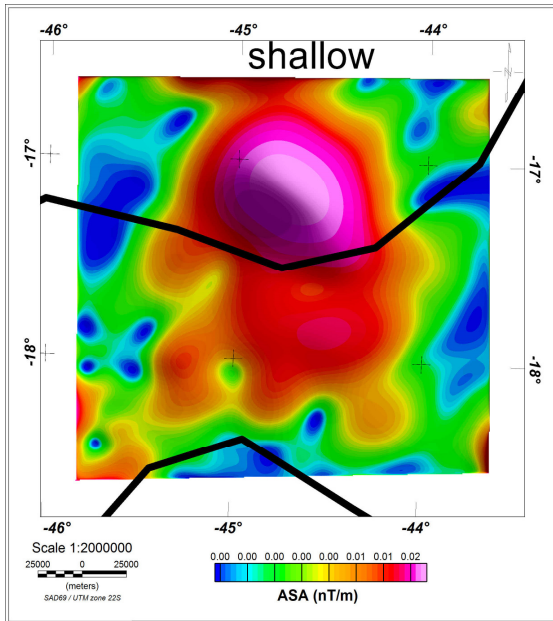


Figure 8 - Regional distribution of analytic signals derived from anomalous magnetic fields for block A in the Pirapora region, obtained by the method of matched filtering. The upper and lower panels indicate fields at depths of 5 and 20 km.

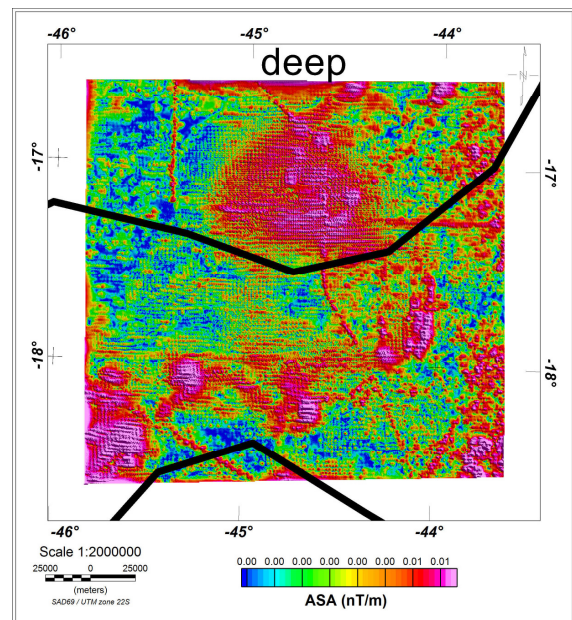
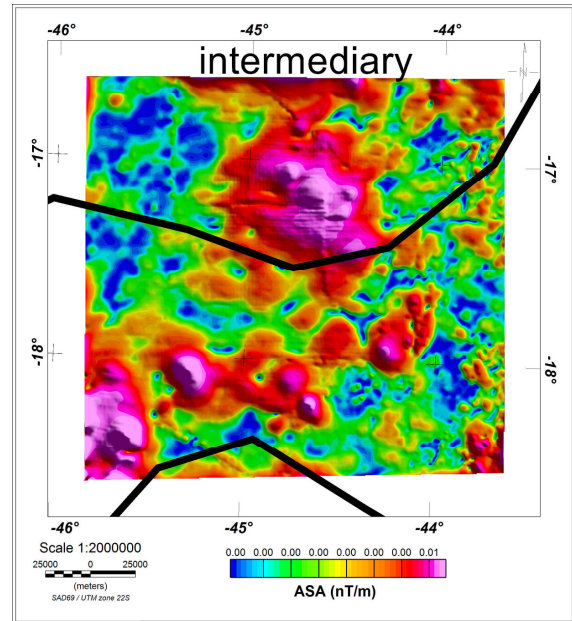


Figure 9 - Regional distributions of analytic signals at intermediate and deeper depths block A in the Pirapora region, obtained by the method of matched filtering. The black curves indicate the limits of the belt identified in figure 7.

8. Implications for Crustal Thermal Field

The results of magnetic data analysis allow inferences as to the geothermal field of Pirapora area. The temperature distributions in the area where the depth to bottom of magnetized bodies extend into the upper mantle is examined in the following sections. The analysis is focused on depths to Curie temperature. In doing so we have also considered depths to curie isotherms of neighboring regions, considered in the previous work of Guimarães et al (2014).

Table 1 - Depths to the top (Z_t) and the bottom (Z_b) of the selected windows for the Pirapora region, based on the matched filtering method of this work. WS refer to window size.

ID	WS (km)	Coordinates		Depth (km)					
		Lon	Lat	Shallow		Intermediate		Deep	
				Z_t	Z_b	Z_t	Z_b	Z_t	Z_b
Blocks within east-west trending belt of figure 1									
C	200	-45,55	-17,74	0,7	1,1	1,8	14,6	15,2	32,7
B	200	-43,67	-18,04	0,9	1,3	1,1	8,8	14,9	34,0
F	300	-46,54	-18,59	0,7	1,3	1,8	8,1	21,6	34,5
E	300	-43,02	-16,67	0,7	1,1	1,2	7,1	18,2	38,3
Blocks north of the east-west trending belt									
D	300	-45,18	-16,16	0,8	1,4	2,1	12,3	19,0	45,8
A	300	-45,12	-16,74	0,8	1,3	1,7	18,8	20,2	53,1
Block south of the east-west trending belt									
G	300	-45,03	-19,44	0,7	1,1	1,5	10,5	15,8	42,6

8.1. Thermal Models

An approximate estimate of the geothermal gradient could be obtained using the values of depth to bottom of magnetized layer (Z_b) and Curie temperature (T_c). However, such estimates do not take into consideration the effect of radiogenic heat in crustal layers. Improved estimates of temperature can be obtained using the relation proposed by Hamza (1982) and Alexandrino (2008). For a medium with temperature dependent thermal conductivity (λ) and exponential decrease of radiogenic heat (A) the relation for heat flow (q) arising from bottom temperature (T_c) and surface temperature (T_0) is:

$$q(z) = \frac{\lambda_0}{z \cdot \alpha} \ln \left(\frac{T_c}{T_0} \right) + A_0 D \left[1 - \frac{(1 - e^{-u})}{u} \right] \quad (5)$$

Where $u = 1 + \alpha T$ (α being the temperature dependence of thermal conductivity), λ_0 the thermal conductivity at temperature at the surface (T_0) and D the logarithmic decrement of heat production with depth surface value of A_0 . The relation for temperature (T) at depth (z) may be obtained from the relation:

$$T_c(z) = \left(\frac{1}{\alpha}\right) \left\{ (1 + \alpha T_0) * e^{\left[\left(\frac{\alpha}{\lambda_0}\right) (q_p z - A_0 D z + A_0 D^2 (1 - e^{-(1-T_c)})\right)]} - 1 \right\} \quad (6)$$

In deriving equations (5) and (6) the physical properties of the medium are assumed to be constant and laterally homogeneous. Table 2 provide a summary of parameter values used in model calculations.

Table 2: Values of Parameters used in geothermal model calculations.

Parameter	Value
Surface temperature (T_0)	25 °C
Thermal conductivity at the surface (λ_0)	2.5 Wm ⁻¹ K ⁻¹
Rate of radiogenic heat production (A_0)	1.1 μWm ⁻³
Logarithmic Decrement (D)	10 km
Temperature Coefficient of thermal conductivity (α)	0.0011 °C ⁻¹
Curie Temperature (T_c)	580 °C

Values of heat flow and geothermal gradients calculated using equation (5) for crustal blocks with depth to Curie point depth lower than 35 km are provided in Table 3, whereas Table 4 provides values for crustal blocks with Curie point depth larger than 35 km.

Figure 10 illustrates the regional distributions of geothermal gradient (upper panel) and heat flow (lower panel) in the region of Pirapora. The dots indicate the center of the blocks (cells) used in spectral analysis. It is clear that gradient values are lower in the central parts of the study area. The zone of gradients with values less than 13.4 °Ckm⁻¹ extends to regions south of Pirapora.

Table 3 - Values of heat flow and geothermal gradients for the crustal blocks with Curie depths less than 35 km. The rows highlighted in green refer to blocks within or adjacent to the Pirapora region.

Block	Long (W)	Lat (S)	Z (Curie-km)	Heat Flow (mW m ⁻²)	Gradient (°C km ⁻¹)
M8	-49,74	-5,77	22,90	55,0	21,99
M7	-49,73	-7,26	25,40	50,5	20,19
M5	-49,98	-12,87	28,30	46,4	18,56
M13	-40,06	-13,01	29,50	44,9	17,95
R6(C)	-45,55	-17,74	32,70	41,4	16,56
M1	-49,53	-9,37	33,00	41,2	16,49
M2	-49,52	-12,08	33,30	40,9	16,37
S2(B)	-43,67	-18,04	34,00	40,3	16,12
T7	-49,4	-14,67	34,30	40,0	16,01
T6(F)	-46,54	-18,59	34,50	39,8	15,93

Table 4 - Values of heat flow and geothermal gradients for the crustal blocks with Curie depths larger than 35 km. The rows highlighted in green refer to blocks within or adjacent to the Pirapora region.

Block	Long (W)	Lat (S)	Z (Curie-km)	Heat Flow (mW/m ²)	Gradient (°C/km)
M6	-50,16	-15,76	36,60	38,1	15,25
M4	-49,19	-16,14	38,10	37,0	14,80
T3 (E)	-43,02	-16,67	38,30	36,9	14,76
V3	-49,41	-10,63	39,80	35,9	14,34
V4	-45,47	-15,61	41,00	35,1	14,05
M12	-41,99	-12,94	42,70	34,1	13,64
T2 (G)	-45,03	-19,44	42,60	34,2	13,67
T1	-42,19	-19,32	44,30	33,2	13,29
T5	-44,02	-20,87	44,40	33,2	13,27
V7(D)	-45,18	-16,16	45,80	32,5	13,00
M14	-42,10	-18,4	46,70	32,1	12,83
V1	-42,16	-11,16	47,70	31,6	12,63
T4 (A)	-45,12	-16,74	53,10	29,4	11,76

A similar trend can also be seen in the distribution of heat flow values (Figure 11). This may be considered as indication that the source of the magnetic anomaly at Pirapora is an intra-crustal feature with roots extending up to depths of 20 to 55 km.

There are indications that the top part of the mantle itself magnetized. According to thermal models of the present work the base of magnetized crust extends to depths greater than the base of the crust in the area of “Pirapora Salience” and surroundings.

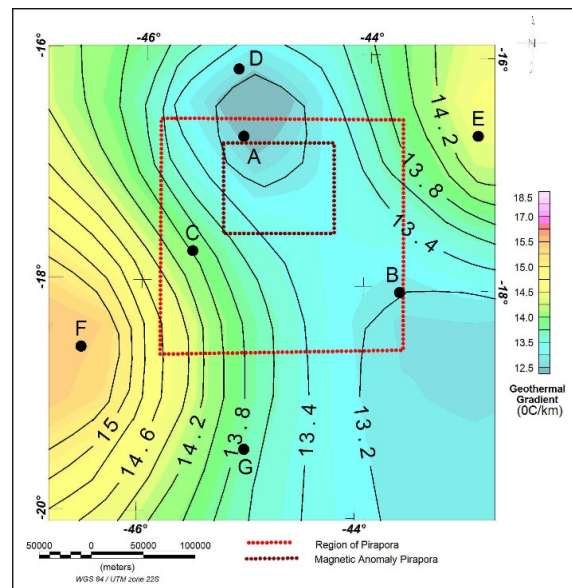


Figure 10 - Regional distributions of geothermal gradient in the region of Pirapora. The dots indicate the center of the blocks (cells) used in spectral analysis

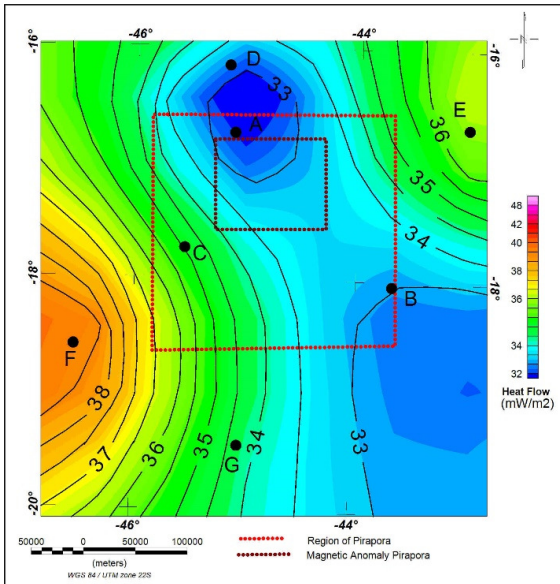


Figure 11 - Regional distributions of heat flow in the region of Pirapora. The dots indicate the center of the blocks (cells) used in spectral analysis.

9. Conclusions

The main residual magnetic anomaly at Pirapora region has values in the range of ± 300 nT and spans over an area of about 9000 square kilometers. Moreover, several small-scale anomalies occur in the south and southwestern part of the study area. The analytic signal has an approximate oval shape and is situated between 44.5° and 45.5° W and between 16.5° and 18.5° S, with a maximum value of about 0.028 nTm $^{-1}$. Results of spectral analysis based on matched bandpass filtering has allowed identification of three layers, which contribute to the magnetic anomaly at the surface. The top layer is situated between 0.7 and 1.4 km while the intermediate layer has depth values in the arrange of 1.4 to 19 km.

The bottom layer is found to have depths lower than the crustal thickness of 35 km, along an east-west trending belt in the Pirapora region. However, in areas to the north and also to the south of this central belt, depth to bottom of magnetic sources have values in excess of 40 km. The obvious conclusion is that the top part of the mantle in these regions are magnetized.

Geothermal model studies have been carried out for investigating the distribution of subsurface temperatures in the local crustal layers. The results indicate that gradient values are relatively low (13-14 $^\circ\text{Ckm}^{-1}$) along the north-south trending belt. This also appears to be true for the local heat flow field, which has values of < 34 mWm $^{-2}$. The main conclusion emerging from geothermal studies is that magnetization extend into the top layer of mantle in the northern and southern segments of the east-west belt of the Pirapora region. Similar results, indicating magnetization of cratonic upper mantle, has also been discussed in some recent works (Chiozzi et al, 2005; Freidman et al, 2014).

Acknowledgments

This study is part of post-doctoral project of the first author at the Department of Geophysics of the National Observatory - ON/MCTI. The second author is recipient of a research scholarship (Process No. 306755/2017-3) granted by the National Research Council of Brazil (CNPq).

References

- Alexandrino, C.H. 2008. Campo termal da província estrutural São Francisco e faixas móveis adjacentes. Tese doutorado em Geofísica. Observatório Nacional, Rio de Janeiro, Brazil, p.184.
- Aisengart, T. 2015. Qualitative and Quantitative Magnetization Vector Inversion applied to the Pirapora Anomaly. 14th International Congress of the Brazilian Geophysical Society, Rio de Janeiro, Brazil, August 3-6.
- Alkmim, F.F., Marshak, S. 1998. Transamazonian orogeny in the Southern São Francisco craton region, Minas Gerais, Brazil: evidence for Paleoproterozoic collision and collapse in the Quadrilátero Ferrífero. *Precambrian Research*, 90(1), 29–58.
- Alkmim F.F., Marshak S., Pedrosa-Soares A.C., Peres G.G., Cruz S.C.P., Whittington W. 2006. Kinematic evolution of the Araçuaí-West Congo orogen in Brazil and África: Nutcracker tectonics during the Neoproterozoic assembly of Gondwana. *Precambrian Research*, 149, 43-64.
- Almeida, F.F.M. 1977. O Cráton do São Francisco. *Revista Brasileira de Geociências*, 7, 349-364.
- Almeida, F.F.M., Hasui Y., Brito Neves B.B., Fuck, R.A. 1981. Brazilian structural provinces: an introduction. *Earth Sci Rev*, 17, 1-19.
- Assumpção, M., An, M., Bianchi, M., França, G., Rocha, M., Barbosa, J.R., Berrocal, J. 2004. Seismic studies of the Brasília Fold Belt at the western border of the São Francisco Craton, central Brazil, using receiver function, surface wave dispersion, and tele-seismic tomography. *Tectonophysics*, 388, 173-185.
- Assumpção, M., Bianchi, M., Juliã, J., Dias, F.L., França, G.S., Nascimento, R., Drouet, S., Pavão, C.G., Albuquerque, D.F., Lopes, A.E. 2013. Crustal thickness map of Brazil: Data compilation and main features. *Journal of South America Earth Sci*, 43, 74-85.
- Bhattacharyya, B.K., Leu, L.K. 1977. Spectral analysis of gravity and magnetic anomalies due to rectangular prismatic bodies. *Geophysics*, 42, 41-50.
- Blakely, R.J. 1996. *Potential theory in gravity and magnetic application*. Cambridge University Press.
- Blakely R.J., Simpson R.W. 1986. Approximating edges of source bodies from magnetic or gravity anomalies. *Geophysics*, 51(7), 1494-1498.
- Borges, A.J., Drews, M.G.P. 2001. Características magnetométricas da bacia do São Francisco em Minas Gerais. In: Pinto C.P., Martins-Neto M.A., A bacia do São Francisco. *Geologia e recursos naturais, Belo Horizonte: SBG-MG*, p. 55–66.
- Borges, A.J., Drews, M.G.P. 2009. Anomalias Aeromagnéticas Notáveis da Bacia do Rio São Francisco, 7th International Congress of the Brazilian Geophysical Society, Rio de Janeiro.
- Borges, A.J. 2013. Relatório Interno CPRM (não publicado a comunidade científica).
- Bosum W. 1973. O levantamento aeromagnético de Minas Gerais e Espírito Santo e sua sequência quanto à estrutura geológica. *Revista Brasileira de Geociências*, 3, 149-159.

- Chiozzi P., Matsushima, Y., Okubo, Y., Pasquale, V., Verdoya, M. 2005. Curie-point depth from spectral analysis of magnetic data in central-southern Europe. *Physics of the Earth and Planetary Interiors*, 152, 267-276.
- Clark, D.A., Tonkins, C. 1994. Magnetic anomalies due to pyrrhotite: examples from the Cobar area, N.S.W., *Australia Journal of Applied Geophysics*, 32, 11-32.
- CODEMIG – Companhia de Desenvolvimento de Minas Gerais. 2013. Mapa Geológico 1:1.000.000. Folha Pirapora - SE.23-X-C-I. Projeto Norte de Minas.
- Friedman, S.A., Feinberg, J.M., Ferré, E.C., Demoryc, F., Martín-Hernández, F., Conder, J.A., Rochette, P., 2014. Craton vs. rift uppermost mantle contributions to magnetic anomalies in the United States interior. *Tectonophysics* 624–625, 15–23.
- Guimaraes, S.N.P., Ravat, D., Hamza, V.M. 2014. Combined use of the centroid and matched filtering spectral magnetic methods in determining thermomagnetic characteristics of the crust in the structural provinces of Central Brazil. *Tectonophysics*, 624-625, 87 - 99.
- Hamza, V.M. 1982. Thermal structure of South America continental lithosphere during Archean and Proterozoic. *Brazilian Journal of Geology*, 12, 135-148.
- Haraly, N.L.E., Hasui, Y. 1985. Interpretation of gravity and magnetic data, Central and Eastern Brazil. In: Hinze W.J. (ed.): *The utility of regional gravity and magnetic anomaly maps*. Society of Exploration Geophysicists, Tulsa, Oklahoma, p. 124-131.
- Hercos, C.M., Martins-Neto, M.A., Danderfer Filho, A. 2008. Arcabouço estrutural da Bacia do São Francisco nos arredores da Serra da Água Fria (MG), a partir da integração de dados de superfície e subsuperfície. *Revista Brasileira de Geociências*, 38 (2 - suplemento), 197-212.
- Marinho, F. 1993. Interpretação dos dados gravimétricos e aeromagnetométricos da porção central da Bacia Proterozóica do São Francisco - noroeste do Estado de Minas Gerais. In: SBG, Simpósio do Cráton São Francisco, 2, Salvador, Salvador, Anais, p.170-172.
- Nabighian, M.N. 1972. The analytic signal of two-dimensional magnetic bodies with polygonal cross-section: its properties and use for automated anomaly interpretation. *Geophysics*, 37(3), 507-517.
- Nabighian, M.N., Grauch V.J.S., Hansen R.O., LaFehr T.R., Li Y., Peirce J.W., Phillips J.D., Ruder, M.E. 2005. The historical development of the magnetic method in exploration. *Geophysics*, 70(6), 33-61.
- Okubo, Y., Graf, R.J., Hansen, R.O., Ogawa, K., Tsu, H. 1985. Curie point depths of the island of Kyushu and surrounding areas, Japan, *Geophysics*, 53, 481–494.
- Phillips, J.D. 1997. Potential-field geophysical software for the PC, version 2.2. U.S. Geological Survey Open-File Report 97-725.
- Roest, W.R., Verhoef, J., Pilkington, M. 1992. Magnetic interpretation using the 3-D analytic signal. *Geophysics*, 57(1), 116-125.
- Santos, M.H.L. 2006. Processamento, Nivelamento e Integração de Levantamento Aerogeofísicos Magnetométricos no Estado de Minas Gerais e sua contribuição à Geologia da Porção Sul do Cráton São Francisco. Dissertação de Mestrado N° 210. Universidade de Brasília. Instituto de Geociências. Brasília – DF.
- Spector, A., Grant, F.S. 1970. Statistical models for interpreting aeromagnetic data. *Geophysics*, 35(2), 293-302.
- Souza Filho, R.G. 1995. O arcabouço estrutural da porção externa da Faixa Araçuaí na Serra do Cabral (MG) e o contraste de estilos deformacionais entre os supergrupos Espinhaço e São Francisco. Dissertação de mestrado, Departamento de Geologia, Escola de Minas, Universidade Federal de Ouro Preto, p. 148.